Structure of two-component lipid membranes on solid support: An x-ray reflectivity study

Eva Nováková, Klaus Giewekemeyer, and Tim Salditt*
Institut für Röntgenphysik, Universität Göttingen, Friedrich-Hund-Platz 1, 37073 Göttingen, Germany
(Received 8 May 2006; revised manuscript received 6 July 2006; published 15 November 2006)

We report an x-ray reflectivity study of phospholipid membranes deposited on silicon by vesicle fusion. The samples investigated were composed of single phospholipid bilayers as well as two-component lipid bilayer systems with varied charge density. We show that the resolution obtained in the density profile across the bilayer is high enough to distinguish two head-group maxima in the profile if the sample is in the phase coexistence regime. The water layer between the bilayer and silicon is found to depend on the lipid surface charge density.

DOI: 10.1103/PhysRevE.74.051911 PACS number(s): 87.16.Dg, 61.10.Kw

INTRODUCTION

Recent studies of solid supported lipid bilayers have demonstrated the potential of x-ray reflectivity to probe the molecular structure of lipid model membranes [1,2]. The density profile across a single bilayer $\rho(z)$ in the fluid state can be retrieved on an absolute scale under physiologically relevant conditions of excess water or buffer solutions. Such systems serve as simple model systems for the much more complex biological counterparts [3], and are also interesting components for biotechnological applications, for example, as biofunctionalized solid surfaces.

Here we use x-ray reflectivity to probe the structure of two-component lipid mixtures, with varied surface charges, both in the fluid and gel phase. Protocols for the deposition of solid supported lipid bilayers by vesicle fusion go back to pioneering work by McConnel [4], and have also been adapted for deposition of charged bilayers [5,6]. Cationic and mixed bilayers on solid surfaces have been used to study the absorption of biomolecules such as DNA with the membrane, mainly by fluorescence microscopy [7]. The lipid molecules self-assemble into bilayers in the presence of a hydrophilic solid support, which stabilize a thin water layer between the support and the bottom leaflet of the bilayer. Here we investigate the effect of the bilayer charge on the water spacing between bilayer and silicon substrate, as well as detailed structural characteristics of mixed two-component bilayers. Structural parameters, such as membrane thickness, area per lipid, water thickness, and the number of water molecules per lipid were calculated directly from an electron density profile of the model bilayers. For this purpose, reflectivity signal above background has been measured up to $q_z \simeq 0.6$ Å^{-1} in the fluid phase and $q_z \simeq 0.7$ Å^{-1} in the gel phase of the bilayers, using synchrotron radiation, while a range of at least 0.3 Å^{-1} and 0.35 Å^{-1} was exploitable in-house. The dynamic range covered in the reflectivity signal was seven orders of magnitude for the in-house sealed tube measurements, and more than eight orders of magnitude at the synchrotron. The bilayer was parametrized by an adaptable number n of Fourier coefficients [8], depending on the q_z range probed. Note, that reflectivity yields the bilayer scattering density profile $\rho(z)$ on an absolute scale without free scaling parameters. The parameters were optimized by a global search using a genetic optimization algorithm (Volker Türck, Optimize 5.0 [9]).

Phase separation and lateral demixing of lipids in model systems has presently attracted increased intention again, in view of the possible functionality in biological membranes associated with lateral heterogeneity. Structural characterization on the molecular scale, capable to probe lipid segregation on the nanometer scale, is however challenging. Here we show that a splitting of the density profile in the headgroup region of mixed bilayers is observed, which we associate with lateral demixing of the two lipid components. We also show that the water layer d_w between silicon and the headgroup of the lower leaflet can be determined with high precision, and is found to vary with bilayer charge density σ.

A further, more technical motivation for the present study was to demonstrate the feasibility of single membrane reflectivity experiments with sealed tube in-house instrumentation. Recent work on x-ray reflectivity from solid-supported bilayers has exclusively concentrated on synchrotron experiments [1,2]. In this work we show that high resolution density profiles obtained from least-square fitting to a parametrized bilayer model can be obtained also with an in-house reflectivity setup using Mo $K\alpha$ radiation to penetrate the excess water above the bilayer. Note that in-house experiments are accessible to a broader research community. Furthermore, beam damage does not pose any problems, e.g., in contrast to intense undulator radiation. Finally, complicated and lengthy measurements in particular addressing lipid-protein interaction and/or complex model systems can be sometimes more easily be addressed in in-house experiments where the beam can be used over several weeks in a row.

EXPERIMENTAL METHOD

Preparation of solid supported bilayers

1,2-dipalmitoyl-*sn*-glycero-3-phosphatidilserine (DPPS), 1,2-dioleoyl-3-trimethylammonium-propane (DOTAP), 1,2-dioleoyl-*sn*-glycero-3-phosphatidilcholine (DOPC), 1,2-dioleoyl-*sn*-glycero-3-phosphatidilserine (DOPS), 1,2-dipalmitoyl-*sn*-glycero-3-phosphatidilcholine (DPPC) were obtained from Avanti Polar Lipids (Alabaster, AL). Hepes

*Electronic address: tsaldit@gwdg.de

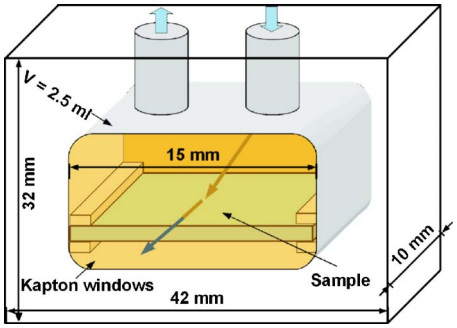

FIG. 1. (Color online) Schematic of the measurement cell.

(H-4034), NaCl (S-9888), sodium dodecyl sulfate (05030), chloroform (25693) were purchased from Sigma-Aldrich (Germany), and $CaCl_2$ from Merck KGaA (Germany). Lipid bilayers were prepared on cleaned (100)-silicon wafers (Silchem, Germany) by vesicle fusion [4,5]. The silicon wafers (15×10 mm) were cleaned by two 20 min cycles of the ultrasonic bath in 2% sodium dodecyl sulfate solution, followed by two 20 min cycles in ultrapure water (18 MΩ cm, Millipore, Bedford, MA), and drying under nitrogen flow. Finally, the surface of the wafers was rendered hydrophilic and cleaned of organic contaminants by etching in plasma cleaner (Harrick Plasma, NY) for 3 min.

A buffer solution (A), made of 150 mM NaCl and 10 mM Hepes, *p*H 7.4 was prepared in ultrapure water and a buffer (B) was prepared by adding 2 mM $CaCl_2$ to the buffer (A).

Lipids were mixed in desired amounts [DPPC/DPPS (molar ratio 4:1, 1:1), DOPC/DOPS (4:1), DOPC/DOTAP (9:1)] and dissolved in chloroform. The solvent was evaporated, followed by drying in a vacuum oven for 24 h in order to remove all traces of solvent. DPPC/DPPS and DOPC/DOPS lipid mixtures were resuspended in a buffer solution (B) at total concentrations 0.75 mg/ml. DOPC/DOTAP lipid mixture was resuspended in 10 mM Hepes solution at total concentration 2.5 mg/ml and DOPC in buffer (A) at the concentration 0.75 mg/ml. Suspensions were vortexed. Small unilamellar vesicles (SUVs) were obtained by sonicating lipid solutions with a tip sonicator (Sonoplus, Germany) for 15–30 min, followed by centrifugation in an Eppendorf centrifuge (10 min at $14.000\times g$) to remove titanium particles. SUV suspensions were stored at 4 °C. Before use, vesicle suspensions, except DOPC/DOTAP, were diluted to final concentrations 0.1 mg/ml.

Cleaned silicon wafers with dimensions 15×10 mm were placed into a chamber with Kapton windows (see Fig. 1), designed for this reflectivity measurement. The chamber frame is made of Teflon that is chemically inert and easy to clean. The x-ray beam enters and exits the chamber through Kapton windows.

The chamber was filled with lipid vesicle solutions and incubated at a room temperature for 30 min. In the case of DOPC/DOTAP lipid mixture the incubation time was 10 h to ensure a symmetric partitioning into both leaflets of the bilayer, which may be kinetically more difficult to achieve for cationic lipids. Excess vesicles were rinsed away, while the membrane remained hydrated all the time during preparation and measurement. The temperature 23.8 °C of the chamber was kept by a flow of 1:2 glycol:water mixture from a temperature-controlled reservoir (Julabo, Germany).

X-ray reflectivity measurements

X-ray reflectivity experiments were performed both at the ID01 undulator beamline (ESRF, Grenoble), using 13.46 keV photon energy, and at a sealed x-ray tube (D8 Advance, Bruker, Germany), operating with Mo $K\alpha$ radiation ($E=17.48$ keV, $\lambda=0.0709$ nm). The in-house reflectometer was equipped with a collimating Göbel mirror system, automatic filters setting and a fast scintillation counter. The beam size in the reflectivity plane was defined by entrance slits to 50 μm. The collimating Göbel mirrors, 50 μm beam size in the scattering plane, and large divergence in the horizontal plane (due to small source-sample distance) optimize signal to noise ratio.

The design of the ID01 beamline is described in detail in Ref. [10]. The incident beam was collimated by various slits. The chamber with the sample was placed on the sample holder horizontally. Intensity of scattered x rays was measured as a function of an incident angle α_i under specular condition (exit angle $\alpha_f=\alpha_i$ and out-of-plane angle $2\theta=0$). The momentum transfer of the elastic scattering $\vec{q}$ was always along q_z, with the z-axis parallel to the sample normal, as illustrated in Fig. 2(a). At both instruments, scans of the x-ray intensity offset from the specular condition (so-called offset scans, obtained from slight detuning to $\alpha_f\neq\alpha_i$) were carried out to correct the data for diffuse background. The beam size was measured precisely for footprint (illumination) correction, and the primary intensity was monitored to obtain the reflectivity on absolute values.

In the full synchrotron beam, radiation damage was observed. We have detected a systematic shift of the minima position, shown in the inset of Fig. 2(b), by measuring a reflectivity around the second minima ($1{,}3°<q_z<1{,}6°$) with increased illumination time. To achieve data sets unspoiled by radiation damage, the following measures were combined: (i) A computer controlled set of attenuators in front of the sample was used, see Fig. 2(b), limiting the full beam exposure only to a selected number of points in the high q_z range. (ii) The sample was translated during illumination in y direction, perpendicularly to the direction of the incident beam and data were always collected from undamaged areas. (iii) A fast shutter system was installed to minimize the exposure time during motor movements. Reproducibility of the measured data was then checked along various parts of the reflectivity curve. The scans were completed in approximately 30 min. For reflectivity measurements carried out at D8 Advance reflectometer, automatic attenuator settings were used. Radiation damage was not observed. The scans were completed in approximately 6 h.

Data treatment

The reflectivity curves were corrected for background (diffuse) scattering, illumination and normalized to primary beam intensity, measured by photodiode monitor. The statistical errors on the measured data points were calculated from Poisson statistics.

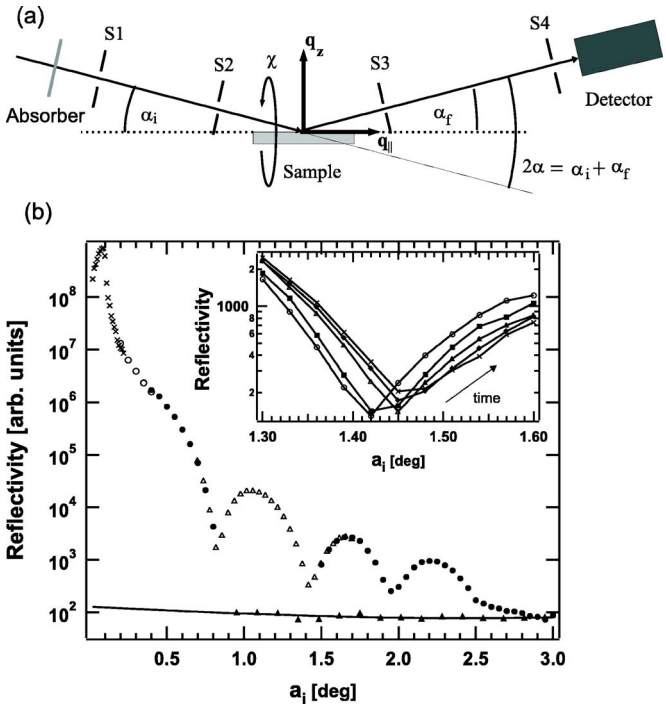

FIG. 2. (Color online) (a) Schematic diagram of the experimental setup. The incident angle α_i is equal to the reflected angle α_f. The only nonzero component of the momentum transfer of the elastic scattering is its z-component q_z, parallel to the sample normal. $S1$-$S4$ denotes slits. (b) X-ray reflectivity scan (before footprint correction) and offset-scan (nonspecular background) of DOTAP/DOPC supported bilayer on silicon wafer, recorded at ID01. Different parts of the reflectivity scan (different symbols) were detected by using the different set of attenuators to prevent radiation damage. Obviously, for smaller α_i, more attenuators were used than for the higher α_i, until removing all attenuators for $q_z \simeq 1.6$ Å^{-1}. Solid line corresponds to the polynomial fit to the measured background. The inset shows the reflectivity curves in the region around the second minima with increasing exposure time using the full beam with no attenuators. The shift in position of the minima [see inset in (b)] as a function of illumination time was already reported in Ref. [2]. This effect can be ascribed to radiation damage, most likely originating from free radical generation by photoelectrons at the solid surface.

The method, we used for data analysis, is based on semikinematical approximation of the reflectivity. The x-ray reflectivity from an interface is characterized by the electron density profile $\rho(z)$ between a medium 1 with electron density ρ_1 and a medium 2 with density ρ_2 and can be expressed by the so-called master formula [11]:

$$R(q_z) = R_F(q_z)\left|\frac{1}{\Delta\rho_{12}}\int \frac{d\rho(z)}{dz}e^{iq_z z}dz\right|^2, \tag{1}$$

where $R_F(q_z)$ is the Fresnel reflectivity of the ideal interface between the two media, q_z is the scattering vector, and $\Delta\rho_{12}$ is the density contrast. In this formalism the $\rho(z)$ is the laterally averaged density profile. $R_F(q_z)$ can be written as $|(q_z - q_z')/(q_z + q_z')|^2$ with $q_z'^2 = q_z^2 - q_c^2$. The critical momentum transfer is directly related to the density contrast by $q_c = 4\pi/\lambda \sin(\alpha_c) \simeq 4\sqrt{\pi r_0 \Delta\rho_{12}}$, with the classical electron radius r_0.

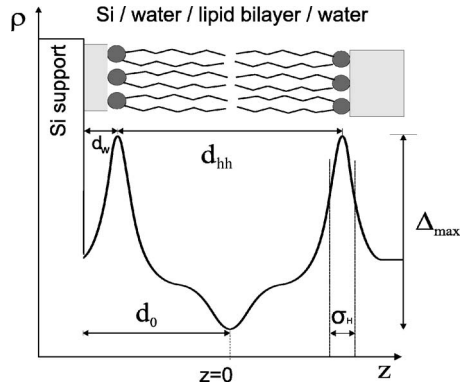

FIG. 3. Model of the electron density profile $\rho(z)$ with the corresponding parameters used in the fitting procedure.

The lipid bilayer is separated from the solid support by a thin water layer [12], as illustrated in Fig. 3. The electron density profile of a lipid bilayer on a Si substrate can be thus written as

$$\rho(z) = (\rho_{\mathrm{Si}} - \rho_{\mathrm{water}})\mathrm{erf}\left(\frac{z + d_0}{\sqrt{2}\sigma}\right) + \rho_0(z), \tag{2}$$

where $(\rho_{\mathrm{Si}} - \rho_{\mathrm{water}})$ corresponds to the contrast of the interface between Si and the thin water layer, corrected by the error function with the rms substrate roughness σ. $\rho_0(z)$ represents the bilayer electron density.

After inserting the electron density profile equation (2) to Eq. (1) and taking the ensemble average, x-ray reflectivity can be written as

$$\begin{aligned} R(q_z) &= R_F(q_z)\left|\int \frac{1}{\sqrt{2\pi\sigma^2}}e^{-(1/2)[(z+d_0)/\sigma]^2}e^{iq_z z}dz \right. \\ &\quad \left. + \frac{1}{\Delta\rho_{12}}\int \frac{\partial\rho_0(z)}{\partial z}e^{iq_z z}dz\right|^2 \\ &= R_F(q_z)|e^{-iq_z d_0}e^{-q_z^2\sigma^2/2} + f(q_z)|^2 \\ &= R_F(q_z)[e^{-q_z^2\sigma^2} - 2ie^{-q_z^2\sigma^2/2}\sin(q_z d_0)f(q_z) + |f(q_z)|^2]. \end{aligned} \tag{3}$$

The first summand represents the reflectivity of the substrate. The second is a cross term and represents interference effects from the substrate with the bilayer. The third summand is the product of the form factor $|f(q_z)|^2$, containing the structural information about the bilayer centered at $z=0$,

$$f(q_z) = \int_{-d/2}^{d/2} \frac{1}{\Delta\rho_{12}}\frac{\partial\rho_0(z)}{\partial z}e^{iq_z z}dz. \tag{4}$$

$\Delta\rho_{12}$ corresponds to the contrast of the water/Si interface, d_0 represents the thickness of a thin water layer with half-membrane thickness (see Fig. 3).

To describe the bilayer density profile $\rho_0(z)$ we chose the parametrization of the bilayer in terms of its first N_0 Fourier coefficients f_n [8],

$$\rho_0(z) = \rho_{\text{water}} + \Delta_{\max}\Delta\rho_{12}\sum_{n=1}^{N_0} f_n v_n \cos\left(\frac{2\pi n z}{d}\right). \quad (5)$$

The term $\left[\Delta_{\max}\Delta\rho_{12}\Sigma_{n=1}^{N_0} f_n v_n \cos\left(\frac{2\pi n z}{d}\right)\right]$ can be understood as a deviation of the electron density of the bilayer from the electron density of surrounding water ρ_{water} in terms of f_n. v_n is the associated (complex) phase factor, which in our case can be shown to reduce to ± 1 only, due to the mirror symmetry of the bilayer. $\Delta_{\max}$ is the amplitude of density deviation to the water density.

The integral of the form factor can be solved analytically after inserting Eq. (5) to Eq. (4), yielding

$$f(q_z) = \sum_{n=1}^{N_0} f_n \Delta_{\max}\left(\frac{i8\pi^2 n^2 \sin(0.5 q_z d)}{q_z^2 d^2 - 4\pi^2 n^2}\cos(n\pi)\right). \quad (6)$$

Finally, the expression (3) was used for the simulation, where the parameters were optimized by a global search using a genetic optimization algorithm (Volker Türck, Optimize 5.0). The fitting procedure results in obtaining the electron density profile on an absolute scale. The fit parameters are reduced to the Fourier coefficients f_n, the associated phase factor v_n, the distance from the substrate to the middle of the bilayer d_0, the critical momentum transfer q_c, the amplitude of density deviation to the water density $\Delta_{\max}$ and the substrate roughness σ. The water electron density was fixed to $0.334e^-/\text{Å}^3$, and the silicon substrate electron density was fixed to $0.699e^-/\text{Å}^3$. The number n of Fourier coefficients is adapted depending on the q_z range, according to $n \simeq \frac{q_{\max}}{2\pi D}$, where D is the width of the film. Thus, the higher the range in momentum transfer $q_{\max}$, the higher the number of the Fourier coefficients (fit parameters) used. The fitting procedure often involves iterative changes in the number of Fourier coefficients.

The main purpose of the electron density profiles is to obtain structural information. The structural parameters can be derived from simple geometric relationships. The highest electron-density peaks on both sides of the centrosymetric electron density profiles $\rho(z)$ of the bilayer coincide with the phospholipid head group ρ_h. The valuable quantity is the separation d_{hh} of these maxima (head-to-head distance), which is a measure of the bilayer thickness. The two side minima correspond to the water layer and the central minimum is associated with the terminal methyl groups of the hydrocarbon chains ρ_c. The thickness of the water layer between Si support and the bilayer, including the water molecules intercalated into the bilayer, can be determined as

$$d_{\text{water}} = d_0 - d_{hh}/2. \quad (7)$$

The area per lipid A is calculated from the relation given by Pabst *et al.* [13],

$$A = \frac{1}{\rho_{\text{CH}_2}\left(\frac{\bar{\rho}_h}{\bar{\rho}_c} - 1\right)}\left(\frac{\frac{\bar{\rho}_h}{\bar{\rho}_c} n_c^e}{d_c} - \frac{n_h^e}{d_h}\right), \quad (8)$$

where n_h^e is the number the head-group electrons and n_c^e number of hydrocarbon electrons. The electron densities of the head-group $\bar{\rho}_h$ and hydrocarbon tails $\bar{\rho}_c$ are defined relatively to the methylene electron density ρ_{CH_2} ($\bar{\rho}_h = \rho_h - \rho_{\text{CH}_2}$, $\bar{\rho}_c = \rho_c - \rho_{\text{CH}_2}$). The methylene electron density, determined from wide-angle diffraction experiments, is $0.317 \pm 0.003 e^-/\text{Å}^3$ [14]. The head-group size d_h is estimated from the full width at half-maximum (FWHM) σ_h of the Gaussian fitted to the head-group region, and the hydrocarbon chain length d_c can be derived from

$$d_c = \frac{d_{hh} - \sigma_h}{2}. \quad (9)$$

The total number of water molecules per lipid molecule between the substrate and the bilayer, including the molecules intercalated into the bilayer, can be estimated from

$$n_w = \frac{A d_w}{V_w}, \quad (10)$$

where $V_w \sim 30$ Å^3 is the volume of one water molecule at 30 °C. We stress, however, that the values for A, n_w, d_c, and d_h are derived from the density profile on the basis of a number of assumptions and definitions, as detailed in Ref. [13]. The primary structural results of the measurement is just the vertical density profile $\rho(z)$.

RESULTS AND DISCUSSION

We measured specular x-ray reflectivity from the various lipid mixtures with low positive [DOPC/DOTAP(9:1)], neutral (DOPC) and negative charge [DOPC/DOPS(4:1), DPPC/DPPS(4:1),(1:1)]. The lipid vesicles were deposited by vesicle fusion on a Si substrate. Experiments were carried out at a constant temperature 23.8 °C. We determined the best fit to the data for each sample by obtaining model intensity curves using the semi-kinematical approach described above. Reasonable starting parameter values were initially set for each fit. The intensity of specularly reflected x rays for lipid mixtures was measured up to the momentum transfer ~0.6 Å for the bilayer in fluid phase and up to ~0.7 Å for the bilayer in gel phase, covering eight orders of magnitude in intensity, before reaching the background level (see Figs. 4 and 5). For reflectivity measurements carried out at D8 Advance reflectometer, we were able to measure intensity of the reflected beam up to the momentum transfer ~0.3 Å for the bilayer in fluid phase and up to ~0.35 Å for the bilayer in gel phase (see Fig. 6).

An estimate of the spatial resolution $d_{\min}$ for the density profile obtained from a reflectivity measurement is given by the sampling theorem $d_{\min} \sim \frac{\pi}{q_{\max}}$, where $q_{\max}$ is the maximum momentum transfer of reflectivity measurement. This would imply $d_{\min} \sim 4.4$ Å (gel phase) and ~5.2 Å (fluid phase) for synchrotron measurements, and approximately 2 times higher values for in-house reflectivity experiments. However, assuming the validity of a given model, for example, the presence of the water layer between substrate and membrane, smaller distances influence the simulation also at smaller q values. However, these results and the corresponding errors follow from the fitting procedure, and are quite model dependent.

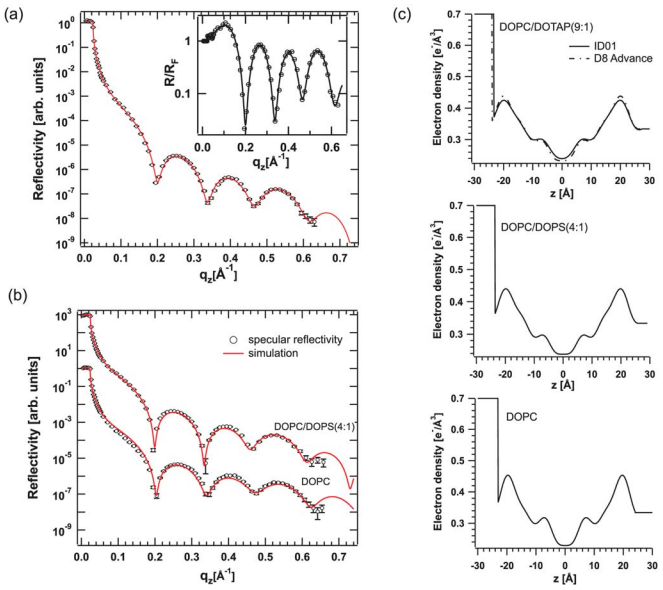

FIG. 4. (Color online) (a,b) The best fit (solid lines) to the reflectivity curves of DOPC/DOTAP(9:1), DOPC/DOPS(4:1) and DOPC in fluid phase at 23.8 °C, recorded at ID01 beamline. The inset gives a reflectivity plotted as R/R_F vs q_z. (c) Electron density profiles corresponding to the simulations in (a,b).

Mixed bilayer in the fluid phase

Figures 4(a) and 4(b) shows the reflectivity curves for DOPC, DOPC/DOPS, and DOPC/DOTAP lipid mixtures as a $\log_{10}$ (reflectivity) vs momentum transfer q_z. The solid curves represent the best fits to the reflectivity.

The main transition temperatures of DOPC, DOTAP, and DOPS are below 0 °C, therefore all compositions of these lipids, we used in our study, are expected to be in the fully hydrated fluid phase at 23.8 °C. The corresponding electron density profiles on the absolute scale ($e^-/\text{Å}^3$) are shown in Fig. 4(c). Derived structural parameters are listed in Table I.

DOPC

The head-to-head distance of the DOPC bilayer was found to be $d_{hh}=39.6$ Å. This can be compared to the value of 37.1 Å for multilamellar DOPC stacks on Si support at 30 °C, given by Liu *et al.* [15]. Leonenko *et al.* [16] measured by AFM the thickness of 40 Å at 22 °C for supported DOPC bilayer deposited on mica.

The water layer thickness between Si substrate and the bilayer was found to be $d_w=4.3$ Å. This is in a good agreement with the value 4 Å for water layer between DOPC bilayer and quartz substrate, reported by Miller *et al.* [1]. The resulting electron density of the lipid heads is estimated to be $\rho_h=0.45e^-/\text{Å}^3$ and the electron density of lipid tails $\rho_t=0.23e^-/\text{Å}^3$. The values compare well to those obtained by diffuse x-ray scattering method [15] and x-ray reflectivity method [17]. The area per lipid has been calculated from Eq. (8). The number of head-group electrons is 164, and the number of hydrocarbon chain electrons is 270 for DOPC. The obtained area per lipid was $A=74.4\pm1.0$ Å^2. For comparison, Petrache *et al.* [18] found $A=72.5$ Å^2 for DOPC in the fluid state at 30 °C.

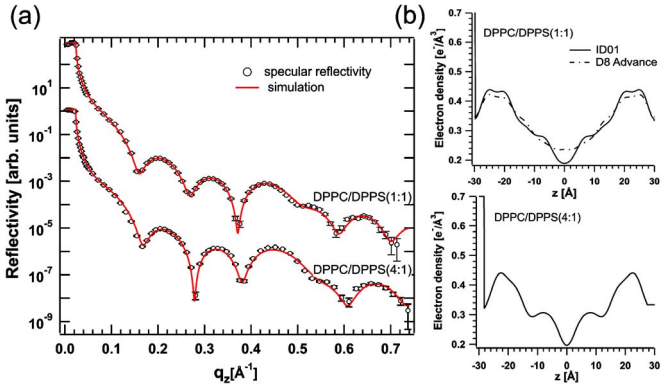

FIG. 5. (Color online) (a) The best fit (solid lines) to the reflectivity curves of DPPC/DPPS(4:1) and DPPC/DPPS(1:1) in gel phase at 23.8 °C, recorded at ID01 beamline. (b) Electron density profiles corresponding to the simulations in (a).

DOPC/DOPS(4:1)

The value, we measured for the head-to-head distance of DOPC/DOPS(4:1) bilayer on silicon support, is $d_{hh}=39.4$ Å, the electron density of lipid tails of $\rho_t=0.24e^-/\text{Å}^3$ and the electron density of lipid heads of $\rho_h=0.44e^-/\text{Å}^3$. We found the thickness of water layer between negatively charged substrate and negatively charged DOPC/DOPS(4:1) membrane to be lower ($d_w=3.9$ Å) than between the substrate and neutral DOPC membrane. The obtained area per lipid was $A=71.1\pm1.3$ Å^2. For the calculation of the number of head-group and hydrocarbon electrons of DOPC/DOPS lipid mixture, we took into the account the molar ratio of DOPC and DOPS in the mixture. The number of head-group electrons is 172 (including the Na^+ ions), and number of hydrocarbon chain electrons is 270 for DOPS. The number of water molecules per lipid molecule between the bilayer and the silicon substrate was found to be approximately $n_w \sim 9.2$ Å. The average area per lipid of DOPC/DOPS mixture was found to be smaller than the area of the DOPC and also n_w is reduced by approximately 1.4 water molecules per lipid. Petrache *et al.* [18] studied structure of charged DOPS bilayer in the fluid state at 30 °C and they reported the value $A=65.3$ Å^2 for DOPS, which is remarkably smaller than their obtained value $A=72.2$ Å^2 for DOPC.

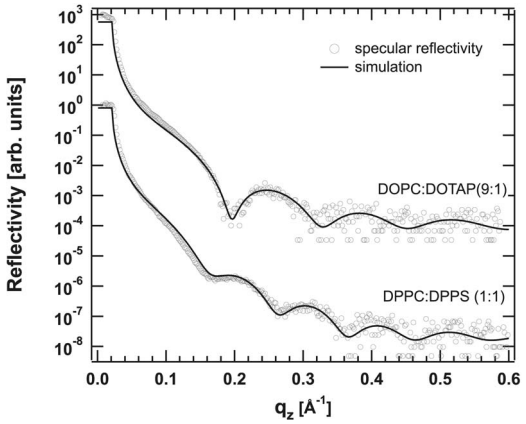

FIG. 6. (Color online) Experimental reflectivities recorded at D8 Advance reflectometer. Solid lines represent the best fit curves.

TABLE I. Derived values for electron density of the head-groups (ρ_h) and of the terminal methyl groups of the hydrocarbon chains (ρ_c), and derived structural parameters calculated by using Eqs. (7)–(10).

Parameter	DOPC	DOPC/DOPS (4:1)	DOPC/DOTAP (9:1)	DOPC/DOTAP (9:1)[a]
$\rho_h(e^-/\text{Å}^3)$	0.45±0.13	0.44±0.05	0.43±0.03	0.44±0.09
$\rho_c(e^-/\text{Å}^3)$	0.23±0.07	0.24±0.03	0.24±0.02	0.23±0.05
d_{hh}(Å)	39.6±0.3	39.4±0.2	39.8±0.2	40.0±1.1
d_w(Å)	4.25±0.23	3.9±0.2	3.4±0.2	3.9±1
d_h(Å)	6.01±0.04	6.30±0.15	6.70±0.15	5.60±0.10
d_c(Å)	16.8±0.15	16.6±0.1	16.5±0.1	17.2±0.55
A(Å^2)	74.4±1.0	71.1±1.3	62.1±0.9	67.2±1.2
n_w	10.6±0.2	9.2±0.2	7.1±0.1	8.7±0.3

[a]Values for D8 Advance measurements.

To enhance bilayer formation from anionic lipids, we have added 2 mM $CaCl_2$ to the buffer solution. It has been reported in the literature, that Ca^{2+} reduces the energy barrier that arises due to electrostatic repulsion between negatively charged substrate and lipids [5,19]. It has been suggested that variations in *p*H, salt concentration, and presence of divalent cations in the fluid phase may change the hydration properties of charged phospholipids [20]. We hypothesize that the effect of a thinner water layer can be due to lower area per lipid of DOPC/DOPS lipid mixture, in contrast to DOPC, or/and due to binding of the bivalent Ca^{2+} ions to negatively charged groups in DOPS.

DOPC/DOTAP(9:1)

For a Si supported DOPC/DOTAP(9:1) membrane we obtained the head-group distance of d_{hh}=39.8 Å, the electron density of the heads of $\rho_h=0.43e^-/\text{Å}^3$, and the electron density of the tails of $\rho_t=0.24e^-/\text{Å}^3$. This compares well to the literature values for DOPC/DOTAP(7:3), given by Yang *et al.* [21]. Molecular dynamics studies have demonstrated DOPC and DOTAP head groups to be located at a similar plane of the bilayer [22] and it was suggested that the quaternary amine of DOTAP and the phosphate group of DOPC may form a salt bridge. Here we find that the head-to-head distances d_{hh} of DOPC/DOTAP mixture and DOPC are similar.

The obtained average area per lipid of DOPC/DOTAP was $A=62.1\pm0.9$ Å^2. For a calculation of the number of head-group and hydrocarbon chain electrons of DOTAP/DOPC mixture, we took into account the molar ratio of DOPC and DOTAP in the lipid mixture. The number of head-group electrons is 112 Hz, and the number of hydrocarbon chain electrons is 270 for DOTAP. The number of water molecules per lipid molecule was found to be $n_w\sim7.1$ Å. We found that the area of DOPC/DOTAP mixture is remarkably smaller than the area 74.1 Å^2 for DOPC, and n_w is reduced approximately by three water molecules per lipid, comparing to the DOPC supported bilayer. The thickness of head-group region $d_h\sim6.7$ Å increased approximately by 0.7 Å, in contrast to DOPC.

Furthermore, we get $d_w\sim3.4$ Å thin water layer between Si support and DOPC/DOTAP(9:1) membrane. This is ~1 Å less, respectively, than the value for DOPC membrane. This reduction of the water layer can be caused by lower area per lipid of DOTAP/DOPC mixture, in contrast to DOPC, or/and it could indicate electrostatic interactions between the low positively charged DOPC/DOTAP(9:1) membrane and the negatively charged silicon support.

Mixed bilayer in the gel phase and lateral demixing

Figure 5(a) shows the reflectivity curves for DPPC/DPPS (4:1, 1:1) lipid mixtures as a $\log_{10}$ (reflectivity) vs q_z. The solid curves represent the best fits to the reflectivity. The phase transitions of DPPC and DPPS from the order gel phase to the disordered liquid-crystalline phase are reported in the literature to occur at 41.4 °C and 54 °C [20]. Therefore, we expect to have DPPC/DPPS mixtures at experimental temperature 23.8 °C in gel phase. The corresponding electron density profiles are shown in Fig. 5(b). The structural parameters are listed in Table II.

DPPC/DPPS(4:1)

From the analysis of the simulation for reflectivity profile of DPPC/DPPS(4:1) bilayer, we obtained the electron density of lipid heads of $\rho_h=0.44e^-/\text{Å}^3$ and the electron density of lipid tails of $\rho_t=0.2e^-/\text{Å}^3$. The thickness of the bilayer was found to be $d_{hh}\sim45$ Å. The obtained average area per lipid was $A=43.3\pm2.6$ Å^2. For the calculation of the number of head-group and hydrocarbon electrons for DPPC/DPPS lipid mixture, we took into account the molar ratio of DPPC and DPPS in the mixture. The number of head-group electrons is 164 for DPPC and 172 for DPPS, and the number of hydrocarbon chain electrons is 242 for DPPC and DPPS. For comparison, Wiener *et al.* [14] measured the values, $\rho_h=0.47e^-/\text{Å}^3$, $\rho_t=0.21e^-/\text{Å}^3$, $d_{hh}=45$ Å, and $A=45.9\pm2.0$ Å^2 for gel phase DPPC bilayer at $T=20$ °C by x-ray scattering methods.

The water layer between the silicon and DPPC/DPPS (4:1) was found to be ~5.7 Å.

DPPC/DPPS(1:1)

In the case of DPPC/DPPS(1:1) bilayer, we observe a splitting of the head-group region into two parts, with the

TABLE II. Derived values for electron density of the head-groups (ρ_h) and of the terminal methyl groups of the hydrocarbon chains (ρ_c), and derived structural parameters calculated by using Eqs. (7)–(10).

Parameter	DPPC/DPPS (4:1)	DPPC/DPPS (1:1)	DPPC/DPPS (1:1)[a]
$\rho_h(e^-/\text{Å}^3)$	0.44±0.03	0.44±0.01 (0.43±0.01)[b]	0.42±0.05
$\rho_c(e^-/\text{Å}^3)$	0.20±0.02	0.19±0.02	0.235±0.030
d_{hh}(Å)	45.0±0.5	49.8±0.1 (41.4±0.08)[b]	49.8±0.7
d_w(Å)	5.7±0.4	4.9±0.2	3.8±0.6
d_h(Å)	13.7±1.6		11.2±0.5
d_c(Å)	15.6±0.8		19.3±0.4
A(Å^2)	43.3±2.6		43.65±1.15
n_w	8.2±0.5		5.5±0.7

[a]Values for D8 Advance measurements.
[b]The values for the second maxima in the electron density profile of the DPPC/DPPS(1:1).

corresponding electron densities of lipid heads $\rho_h = 0.44e^-/\text{Å}^3$ and $\rho_h^* = 0.43e^-/\text{Å}^3$, and with the head-group separations of $d_{hh}=49.8$ Å and $d_{hh}^*=41.4$ Å, respectively. We hypothesize that this separation in the head-group region is likely to be caused by calcium-induced lipid segregation in the film. However, more experiments are needed to verify lateral segregation.

Ohnishi and Ito [23] observed calcium-induced clustering of PC molecules in PS/PC membrane. PS molecules, on the other hand, form solid aggregates bridged by intermolecular calcium chelation, causing motional freezing of lipids. They concluded, that the motional freezing results from closer packing of lipid molecules in the bilayer structure. The closer packing of lipid molecules could explain our observation of the larger distance between two outer head-group maxima in the electron density profile of the DPPC/DPPS(1:1) bilayer, $d_{hh}=49.8$ Å, comparing with the head-group distance of DPPC/DPPS(4:1) bilayer of $d_{hh}=45$ Å. We hypothesize, that the structure of $\rho(z)$ reflects the following components (after lateral average in the plane of the bilayer): the water layer, an outer head-group region of closely packed DPPS molecules, DPPS tails with DPPC head-groups and mixed tails of DPPC and DPPS molecules.

Ohnishi and Ito [23] furthermore noted, that the motive force for the phase separation is formation of Ca-PS aggregates in the bilayer. Jacobson *et al.* [24] found out, that Ca^{2+} ions added to mixed bilayers can induce lateral phase separation isothermally, with the neutral PC molecules segregating from acidic PS. They observed, that calcium ions do not induce phase separation below a critical concentration and, then only with mixtures containing more than 50% PS. This could explain, why we did not observe the segregation of lipids in DPPC/DPPS(4:1) supported bilayer. Another explanation would be a possibly insufficient resolution to detect the separation in DPPC/DPPS(4:1) mixture. Note that Ross *et al.* [25] have imaged calcium-induced domains in DPPC/DPPS(4:1) by AFM in Langmuir-Blodgett layers in the presence of 0.1 mM $CaCl_2$. They observed, that even negligibly small traces of calcium ions present in the buffer solution lead to their accumulation at negatively charged lipid domains.

The thickness of the water layer between DPPC/DPPS (1:1) bilayer and the silicon support ($d_w \sim 4.9$ Å) was reduced, compared to DPPC/DPPS(4:1) bilayer. The thinning of the water layer could be explained by increased attractive electrostatic forces between negatively charged substrate and the DPPC/DPPS(1:1) bilayer, caused by the higher concentration of Ca^{2+} ions binding to the lipid head-groups. The average area per lipid obtained by in-house experiment was $A=43.65\pm1.15$ Å^2 for DPPC/DPPS(1:1) lipid mixture.

For completeness, we summarize all the resulting fit parameters in Table III.

SUMMARY AND CONCLUSIONS

Let us briefly compare structural analysis using single supported bilayers, multilamellar thin films, and multilamellar liposome suspensions (probed by bulk SAXS). In all three cases, a wide q_z-range can be measured and analyzed by full q_z-fitting [8,13,26]. However, multilamellar bilayer suspension undergo much stronger thermal fluctuations, in particular in bulk phases, while the presence of the flat substrate quenches the thermal fluctuations on long lateral length scales leading to an enhanced resolution in $\rho(z)$. This is an advantage in using solid supported membranes, either single bilayers or stacks. Furthermore the membranes can be investigated along both symmetry axis perpendicular or lateral independently [27,28]. While thick stacks provide the large scattering volume needed for lateral structure analysis, specular reflectivity is as easily carried out on aligned stacks as on single bilayers. Stacks require a precise modeling of the structure factor including effects of thermal interbilayer positional fluctuations and coverage [26], while the analysis of single bilayers is more rapid and it is significantly easier to achieve high quality fits. Single bilayer reflectivity also allows for the highest resolution obtainable in the fluid state and at full hydration. Furthermore, we have shown that such analysis does not rely only on synchrotron radiation, but can

TABLE III. Fit results for different lipid mixtures at 23.8 °C (also see Fig. 3).

Fit parameter	DOTAP/DOPC (1:9)	DOPC/DOPS (4:1)	DOPC	DPPC/DPPS (4:1)	DPPC/DPPS (1:1)	DOTAP/DOPC[a] (1:9)	DPPC/DPPS[a] (1:1)
$f1$	−0.92	−0.93	−0.70	−0.75	−0.75	−0.93	−0.7
$f2$	−0.70	−0.71	−0.67	−0.36	−0.19	−0.70	−0.18
$f3$	0.36	0.40	0.33	0.28	0.11	0.36	0.14
$f4$	−0.15	−0.12	−0.20	−0.4	−0.2	−0.16	−0.08
$f5$	−0.28	−0.28	−0.36	−0.07	0.01	−0.25	0.06
$f6$	0.08	0.1	0.1	−0.1	−0.05	0.10	−0.04
$f7$	−0.1	−0.09	−0.06	0.02	0.03	−0.1	0.02
$f8$	0.05	0.04	0.02	0.01	−0.05	0.05	−0.04
$f9$	0.05	0.1	0.11	−0.05	0.05	0.09	0.04
$d0$	23.32±0.12	23.56±0.10	23.05±0.18	28.26±0.34	29.8±0.06	23.98±0.63	28.74±0.40
qc	0.0245±0.0003	0.0242±0.0006	0.0238±0.0001	0.0233±0.0007	0.0237±0.0001	0.0217±0.0001	0.0216±0.0004
Δ_{max}	0.16±0.01	0.18±0.02	0.20±0.06	0.27±0.02	0.38±0.01	0.18±0.04	0.35±0.04
σ	2.04±0.08	2.05±0.18	1.40±0.66	2.46±0.10	2.09±0.14	2.04±0.47	5.42±0.28

[a]Values for D8 Advance reflectometer measurements.

also be carried out at sealed tube instruments with optimized equipment. We have shown that the resolution is high enough to detect a splitting in the head-group maximum, which we attribute to lateral demixing of the two-component system. Diffuse x-ray scattering can be used in future to support this conclusion and to determine the lateral size of the domains. On the other hand, the presence of the substrate may lead to distortions and small structural changes of the bilayer. The water layer d_w between silicon and the head-group of the lower leaflet can be determined with high precision, and is quite small $d_w \leqslant 6$ Å for all samples, indicating that the bilayers are rather close to the solid surface. The system can thus be regarded as a pinned bilayer, in contrast to the free floating membranes, which can be achieved by preparation of a bilayer on top of a monolayer [29,30].

ACKNOWLEDGMENTS

The authors are grateful to Hartmut Metzger and Peter Boesecke for providing optimum working conditions at ID01 beamline, and ESRF for beamtime. The authors acknowledge the EU for funding via the SOFTCOMP network of excellence.

[1] C. E. Miller, J. Majewski, T. Gog, and T. L. Kuhl, Phys. Rev. Lett. **94**, 238104 (2005).
[2] C. Reich, M. B. Hochrein, B. Krause, and B. Nickel, Rev. Sci. Instrum. **76**, 095103 (2005).
[3] E. Sackmann, Science **271**, 5245 (1996).
[4] T. H. Watts, A. A. Brian, J. W. Kappler, P. Marrack, and H. M. McConnell, Proc. Natl. Acad. Sci. U.S.A. **81**, 7564 (1984).
[5] R. Richter, A. Mukhopadhyay, and A. Brisson, Biophys. J. **85**, 3035 (2003).
[6] I. Reviakine and A. Brisson, Langmuir **16**, 1806 (2000).
[7] B. Maier and J. O. Rädler, Phys. Rev. Lett. **82**, 1911 (1999).
[8] T. Salditt, C. Li, A. Spaar, and U. Mennicke, Eur. Phys. J. E **7**, 105 (2002).
[9] http: //sol.physik.tu-berlin.de/htm_trk/.
[10] S. Lequien, L. Goirand, and F. Lesimple, Rev. Sci. Instrum. **66**, 1725 (1995).
[11] J. Als-Nielsen and D. McMorrow, *Elements of Modern X-Ray Physics* (Wiley, Chichester, 2001).
[12] B. W. Koenig, S. Krueger, W. J. Orts, C. F. Majkrzak, N. F. Berk, J. V. Silverton, and K. Gawrisch, Langmuir **12**, 1343 (1996).
[13] G. Pabst, M. Rappolt, H. Amenitsch, and P. Laggner, Phys. Rev. E **62**, 4000 (2000).
[14] M. C. Wiener, R. M. Suter, and J. F. Nagle, Biophys. J. **55**, 315 (1989).
[15] Y. Liu and J. F. Nagle, Phys. Rev. E **69**, 040901(R) (2004).
[16] Z. V. Leonenko, E. Finot, H. Ma, T. E. S. Dahms, and D. T. Cramb, Biophys. J. **86**, 3783 (2004).
[17] M. B. Hochrein, C. Reich, B. Krause, J. O. Rädler, and B. Nickel, Langmuir **22**, 538 (2006).
[18] H. I. Petrache, S. Tristram-Nagle, K. Gawrisch, D. Harries, V. A. Parsegian, and J. F. Nagle, Biophys. J. **86**, 1574 (2004).
[19] F. F. Rossetti, M. Bally, R. Michel, M. Textor, and I. Reviakine, Langmuir **21**, 6443 (2005).
[20] *Phospholipids Handbook*, edited by G. Cevc, 2nd ed. (Marcel Dekker, New York, 1993).
[21] L. Yang, H. Liang, T. E. Angelini, J. Butler, R. Coridan, J. X. Tang, and G. C. L. Wong, Nat. Mater. **3**, 615 (2004).
[22] N. J. Zuidam and Y. Barenholz, Biochim. Biophys. Acta **1329**, 211 (1997).
[23] S. Ohnishi and T. Ito, Biochemistry **13**, 881 (1974).
[24] K. Jacobson and D. Papahadjopoulos, Biochemistry **14**, 152

(1975).
[25] M. Ross, C. Steinem, H. J. Galla, and A. Janshoff, Langmuir **17**, 2437 (2001).
[26] D. Constantin, U. Mennicke, C. Li, and T. Salditt, Eur. Phys. J. E **12**, 283 (2003).
[27] T. Salditt, Curr. Opin. Struct. Biol. **13**, 467 (2003).
[28] Y. Lyatskaya, Y. Liu, S. Tristram-Nagle, J. Katsaras, and J. F. Nagle, Phys. Rev. E **63**, 011907 (2001).
[29] J. Daillant, E. Bellet-Amalric, A. Braslau, T. Charitat, G. Fragneto, F. Graner, S. Mora, F. Rieutord, and B. Stidder, Proc. Natl. Acad. Sci. U.S.A. **102**, 11639 (2005).
[30] G. Fragneto, T. Charitat, F. Graner, K. Mecke, L. Perino-Gallice, and E. Bellet-Amalric, Europhys. Lett. **53**, 100 (2001).